Supplementary information for

Highly Sensitive Surface-Enhanced Raman Scattering Based On Multi-Dimensional Plasmonic Coupling in Au/Graphene/Ag Hybrids

Yuan Zhao,[a] Wencong Zeng,[a] Zhuchen Tao,[a] Penghui Xiong,[b] Yan Qu[c] and Yanwu Zhu*[ad]

[a]Department of Materials Science and Engineering & CAS Key Laboratory of Materials for Energy Conversion, University of Science and Technology of China, Hefei 230026, China

Email: zhuyanwu@ustc.edu.cn

[b]Department of Precision Machinery and Precision Instrumentation, University of Science and Technology of China, Hefei, 230026, China

[c]Wuxi Graphene Technologies Co., Ltd, 311 Yanxin Rd, Wuxi 214174, & China Jiangnan Graphene Research Institute, 6 Xiangyun Rd, Changzhou 213149, China

[d]Collaborative Innovation Center of Chemistry for Energy Materials (2011-iChEM), Hefei 230026, China

Experimental section

Materials

Graphene was grown on copper foils with 25 μm-thickness by atmospheric pressure chemical vapor deposition (CVD) at ~1000 °C using methane as carbon source.[1] Rhodamine B (RhB) and Rhodamine 6G (R6G) and trinitrotoluene (TNT) were purchased from Sigma-Aldrich. All of these reagents were used without further purification. Ultrapure water (18.2 MΩ) was produced using a water purification system (MERCK Millipore Direct-Q3) and used for all aqueous solution preparations.

Preparation of Au NPs/graphene/Ag NPs sandwiched structures

Ag films were deposited at a rate of about 1 Å/s and a pressure of about 10^{-3} Pa by

plasma sputtering.[2-4] Ag NPs were obtained by annealing Ag films in argon atmosphere with a flowing rate of 100 sccm at 300°C for 100 min in a quartz tube furnace. Monolayer graphene films grown on Cu foils were then wet-transferred onto the surface of Ag NPs using Poly(methyl methacrylate) (PMMA).[1] For transfer, PMMA film was first spin-coated onto the surface of graphene on Cu foils and dried at 170°C for 30 min. The PMMA/graphene/Cu foil was then immersed in ammonium persulfate (0.07 g/mL) to etch away the Cu foils, followed by rinsing with deionized (DI) water and soaking in DI water, and then transferred onto the Ag NPs prepared. Finally the PMMA was dissolved with acetone and further treated in flowing Ar to remove PMMA residues, forming graphene-covered Ag NPs films. Au NPs were obtained using the same method as depositing and annealing Ag films aforementioned, resulting in the formation of Au/NPs/graphene/Ag NPs sandwiched hybrid films.

Characterization and instructions

Scanning electron microscopy (SEM, JSM-6700F), atomic force microscopy (AFM, Seiko SP3800) were used to characterize the morphology of Ag NPs, graphene-covered Ag NPs, Au NPs/Ag NPs and Au NPs/graphene/Ag NPs sandwich structures. Absorption spectra of Ag NPs, Au NPs, Au NPs/Ag NPs and Au NPs/graphene/Ag NPs films were measured using a Shimadzu Solid 3700 spectrometer. Optical photographs were taken by a Pentax k-x digital camera.

Raman detection

For measuring the Raman signals of molecules, a 10 μL droplet was dispersed on the as-prepared substrates and dried in air. Raman spectra and mapping were conducted using a Renishaw inVia Raman Microscope. The Raman spectra were recorded using a 532 nm laser with 1 mW laser power and a ×50 objective with 1μm^2 spot. Spectral analysis was performed with a grating of 1800 lines per mm. All Raman spectra were obtained using a linearly polarized laser beam orientated in the x-axis with an integration time of 1 s. The Raman imaging is processed by WiRE 4.3 Raman

software. The SERS EF is calculated by $EF=(I_{SERS}/I_{bulk})\times(N_{bulk}/N_{SERS})$,[3, 5, 6] where I_{SERS} and I_{bulk} are the peak intensities of 10^{-10} M for RhB and R6G or 10^{-11} M for TNT on the 8 nm Au/1LG/8 nm Ag and 10^{-1} M on a quartz substrate at 1649 cm^{-1} (for RhB), 612 cm^{-1} (for R6G) or 1360 cm^{-1} (for TNT), N_{SERS} or N_{bulk} is the number of RhB, R6G or TNT molecules excited by the laser beam on the sandwiched hybrid film or on the quartz, respectively.

FEM simulations

The 3D numerical simulations were performed using Comsol 4.3a, which is based on the finite element method (FEM) to solve Maxwell's equations and to obtain the electric field distribution.[4, 7-9] The simulation configuration is depicted in Fig. 2c. In the vertical direction we set the perfectly-matched-layer (PML) to achieve absorbing boundary conditions, and in the horizontal directions we used periodic boundary conditions to stand for an infinite Au and Ag NPs array.[10, 11] Here, the diameter of both Au and Ag NPs was set as 48 nm (mimicking the 8 nm Ag or Au), and the thickness of monolayer graphene was set as 1 nm (this value is reasonable for CVD-grown graphene if we consider the inhomogeneity caused by the growth and transfer).[12] The dielectric constants of Au and Ag were calculated using Drude model[13] and the complex refractive index $n=3+c_1(\lambda/3)i$ (c_1=5.446 μm^{-1} and λ was the wavelength) was used for graphene.[14] The mesh maximum element size was set as 0.2 nm in the domains representing the graphene, 3 nm in Au NPs and 6 nm for all the elements in the air and substrate subdomains.

For the structure we investigated in the work, the absorption is related to the electric field and the absorption cross-section can be described as[3, 12, 15]

$$\sigma_{abs} = \frac{2\pi}{\lambda A}\int \varepsilon''(\lambda)\left|E(\lambda)\right|^2 dV, \quad (1)$$

where λ is the incident wavelength, A is the area of unit cell, $\varepsilon''(\lambda)$is the imaginary of wavelength dependent relative permittivity, $E(\lambda)$ is the electric field, and the

integration is carried out over the whole volume. That is, the absorption is proportional to the squared electric field enhancement, $|E|^2$.

In SERS, the electric field enhancement is the dominant contribution to the Raman enhancement and the EF can be estimated by[3, 12, 16, 17]

$$I \propto \frac{|E_t|^4}{|E_i|^4}, \quad (2)$$

where E_i is the incident electric field and E_t is the electric field at the location of molecules to be detected.

Thus, both the absorption and the EF can be improved by enhancing the electric field, and the strong absorption may lead to enhanced Raman signals.[18] The absorption of bare metal NPs is caused by the excitation of surface plasmon, and the absorption can be further improved in Au NPs/graphene/Ag NPs hybrids due to the enhanced coupling in the graphene-plasmonic hybrid systems with enhanced light-matter interactions.[11, 12] Compared to Au NPs/graphene/Ag NPs hybrids，the weak Raman sensitivity from bare metal NPs may be related to the weak light absorption.

Notes and references

1. X. Li, W. Cai, J. An, S. Kim, J. Nah, D. Yang, R. Piner, A. Velamakanni, I. Jung, E. Tutuc, S. K. Banerjee, L. Colombo and R. S. Ruoff, *Science*, 2009, **324**, 1312-1314.
2. Plasma Sputter Coating. *http://www.mtixtl.com/desk-topplasmasputteringcoaterformetallic-coatingwithvacuumpumpandgoldtarget15maxsample.aspx*, MTI Corporation.
3. Y. Zhao, X. Li, Y. Du, G. Chen, Y. Qu, J. Jiang and Y. Zhu, *Nanoscale*, 2014, **6**, 11112-11120.
4. Y. Zhao, G. Chen, Y. Du, J. Xu, S. Wu, Y. Qu and Y. Zhu, *Nanoscale*, 2014, **6**, 13754-13760.
5. L. Zhang, C. Jiang and Z. Zhang, *Nanoscale*, 2013, **5**, 3773-3779.
6. W. Fan, Y. H. Lee, S. Pedireddy, Q. Zhang, T. Liu and X. Y. Ling, *Nanoscale*, 2014, **6**, 4843-4851.
7. *COMSOL 4.3a Reference Manual*, 2012, **4.3**.
8. Y. Zhao, X. Hu, G. Chen, X. Zhang, Z. Tan, J. Chen, R. S. Ruoff, Y. Zhu and Y. Lu, *Phys. Chem. Chem. Phys.*, 2013, **15**, 17118-17125.
9. Y. Zhao, G. Chen, Z. Tao, C. Zhang and Y. Zhu, *RSC Adv.*, 2014, **4**, 26535-26542.
10. F. Schedin, E. Lidorikis, A. Lombardo, V. G. Kravets, A. K. Geim, A. N. Grigorenko, K. S. Novoselov and A. C. Ferrari, *ACS Nano*, 2010, **4**, 5617-5626.
11. Y. Du, Y. Zhao, Y. Qu, C.-H. Chen, C.-M. Chen, C.-H. Chuang and Y. Zhu, *J. Mater. Chem. C*, 2014, **2**, 4683-4691.
12. X. Zhu, L. Shi, M. S. Schmidt, A. Boisen, O. Hansen, J. Zi, S. Xiao and N. A. Mortensen,

Nano Lett., 2013, **13**, 4690-4696.
13. E. J. Zeman and G. C. Schatz, *J. Phys. Chem.*, 1987, **91**, 634-643.
14. M. Bruna and S. Borini, *Appl. Phys. Lett.*, 2009, **94**, 031901.
15. N. Reckinger, A. Vlad, S. Melinte, J.-F. Colomer and M. Sarrazin, *Appl. Phys. Lett.*, 2013, **102**, 211108.
16. W. Xu, N. Mao and J. Zhang, *Small*, 2013, **9**, 1206-1224.
17. W. Xu, X. Ling, J. Xiao, M. S. Dresselhaus, J. Kong, H. Xu, Z. Liu and J. Zhang, *Proc. Natl. Acad. Sci. U. S. A.,*, 2012, **109**, 9281-9286.
18. G. Lu, H. Li, C. Liusman, Z. Yin, S. Wu and H. Zhang, *Chem. Sci.*, 2011, **2**, 1817-1821.

Supporting figures

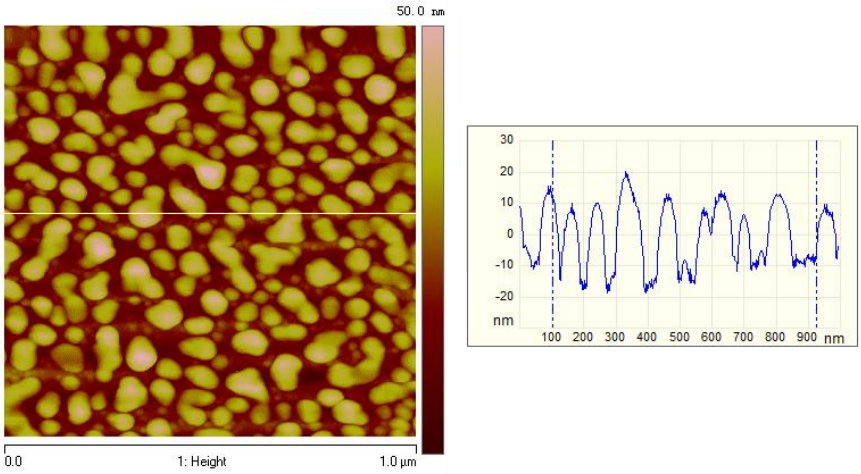

Fig. S1 AFM image and cross-section along the white line for 8 nm Ag (formed by annealing 8 nm-thick Ag film) sample. The average diameter and height for 8 nm Ag are 48 nm and 30 nm, respectively.

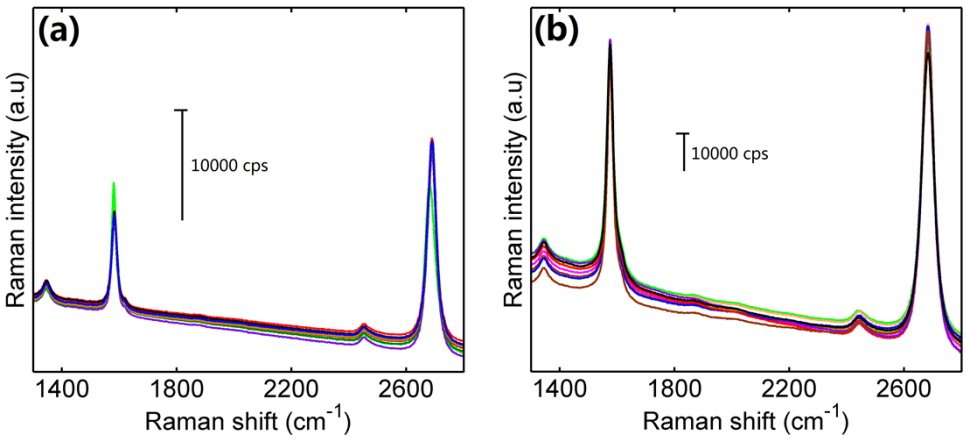

Fig. S2 Raman spectra of monolayer graphene (a) on 8 nm Ag and (b) embedded between 8 nm Au and 8 nm Ag collected from 10 random spots.

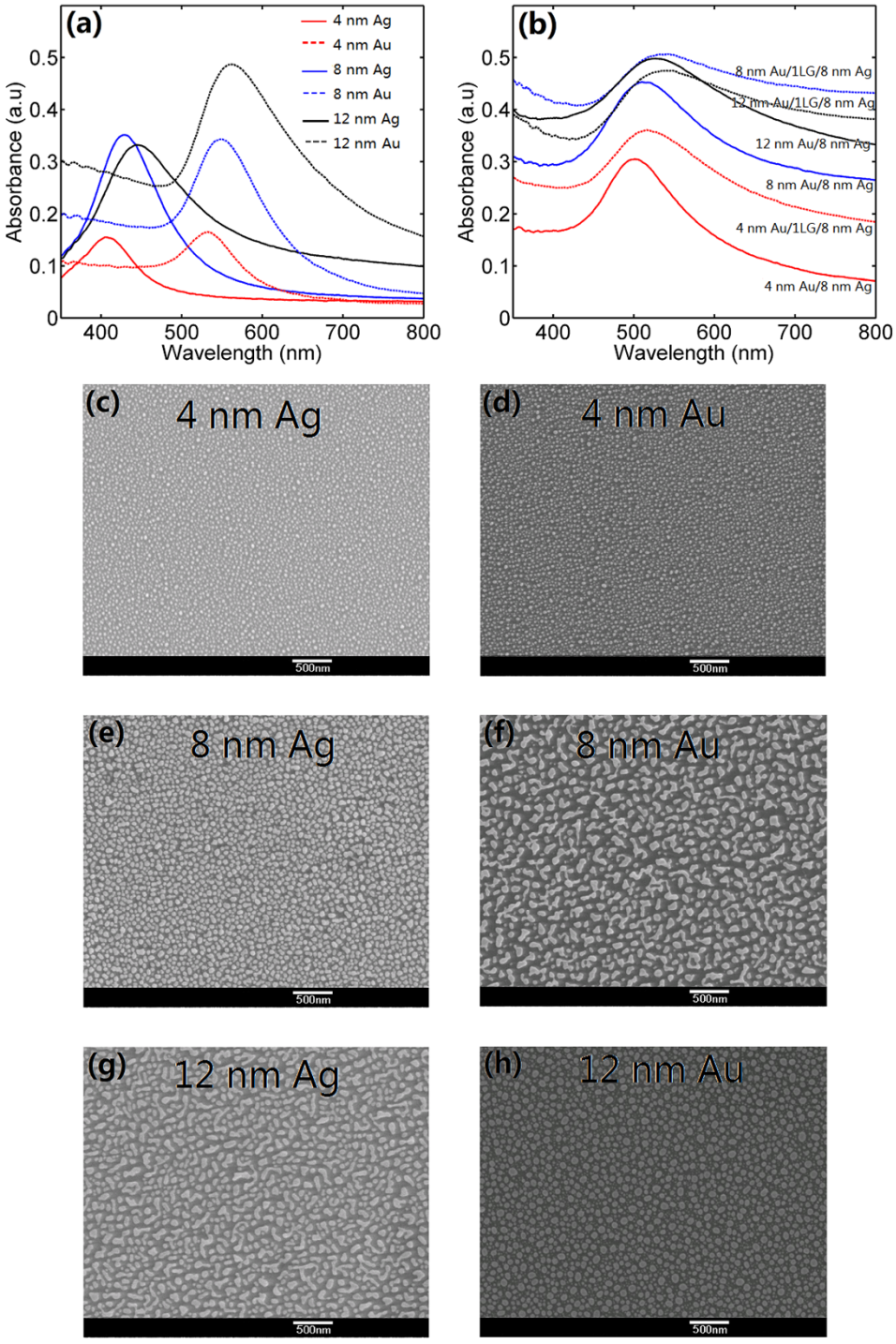

Fig. S3 (a) Absorption spectra for 4 nm (red lines), 8 nm (blue lines) and 12 nm (black lines) Ag (solid lines) and Au (dotted lines) on quartz substrates. (b) Absorption spectra for 4 nm Au/8 nm Ag (red solid lines), 4 nm Au/1LG/8 nm Ag (red dotted lines), 8 nm Au/8 nm Ag (blue solid lines), 8 nm Au/1LG/8 nm Ag (blue dotted lines), 12 nm Au/8 nm Ag (black solid lines) and 12 nm Au/1LG/8 nm Ag (black dotted lines), respectively. SEM images of (c) 4 nm Ag, (d) 4 nm Au, (e) 8 nm Ag, (f) 8 nm Au, (g) 12 nm Ag and (h) 12 nm Au, respectively. The scale bar is 500 nm.

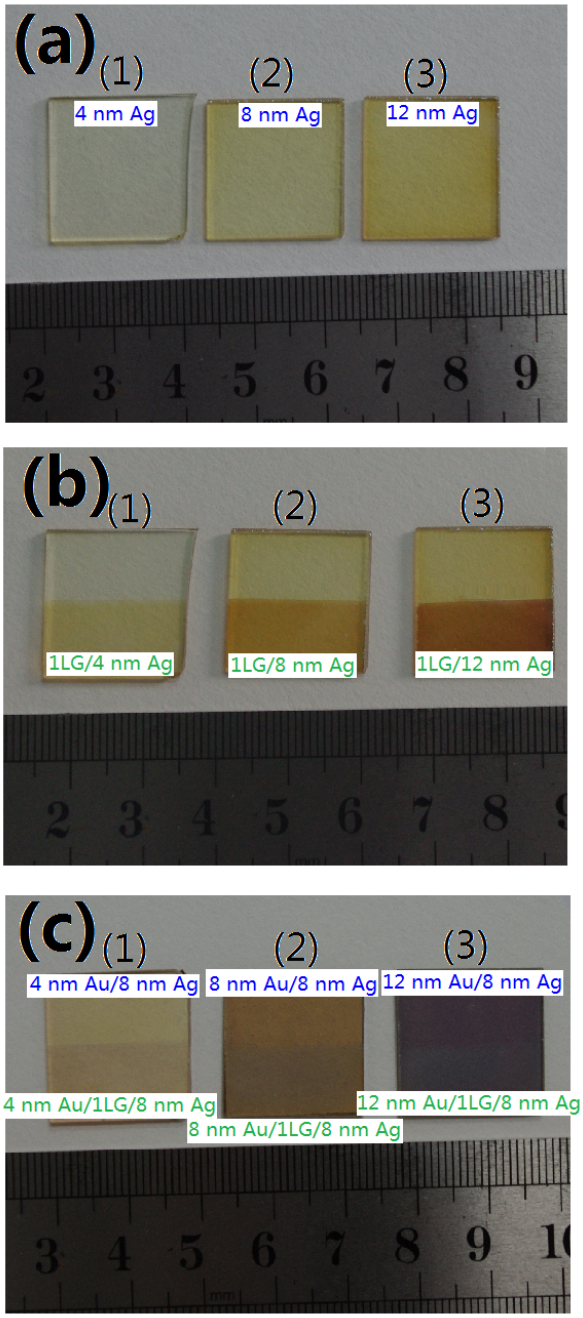

Fig. S4 (a) Optical images of 4 nm Ag (1), 8 nm Ag (2) and 12 nm Ag (3) on quartz substrates. (b) Optical images of monolayer graphene-covered 4 nm Ag (1), 8 nm Ag (2) and 12 nm Ag (3), showing both the bare Ag (upper regions) and graphene-covered (bottom regions) regions. (c) Optical images of 4 nm Au/1LG/8 nm Ag, 8 nm Au/1LG/8 nm Ag (2) and 12 nm Au/1LG/8 nm Ag (3), showing both the graphene embedded regions (bottom regions) and the regions without graphene embedded (upper regions).

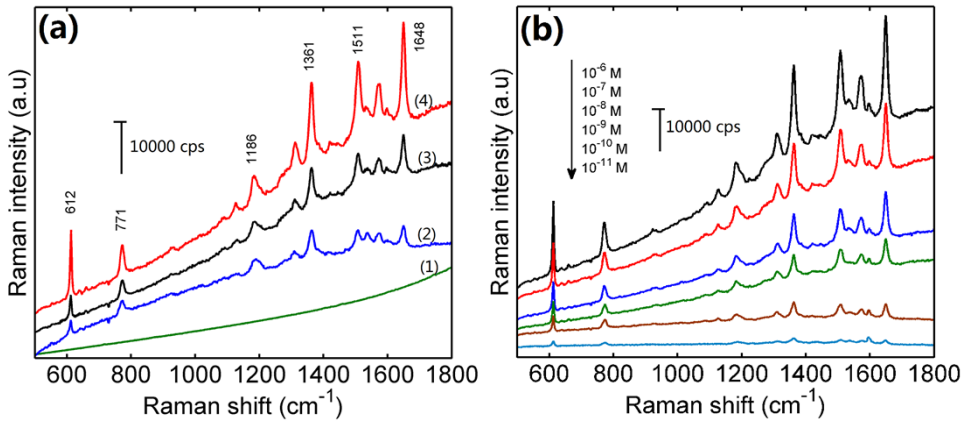

Fig. S5 (a) Raman spectra of 10^{-7} M R6G on quartz (Curve 1), 8 nm Ag (Curve 2), 8 nm Au/8 nm Ag (Curve 3) and 8 nm Au/1LG/8 nm Ag (Curve 4), respectively. (b) SERS spectra of R6G on 8 nm Au/1LG/8 nm Ag structure with 6 different molecular concentrations.

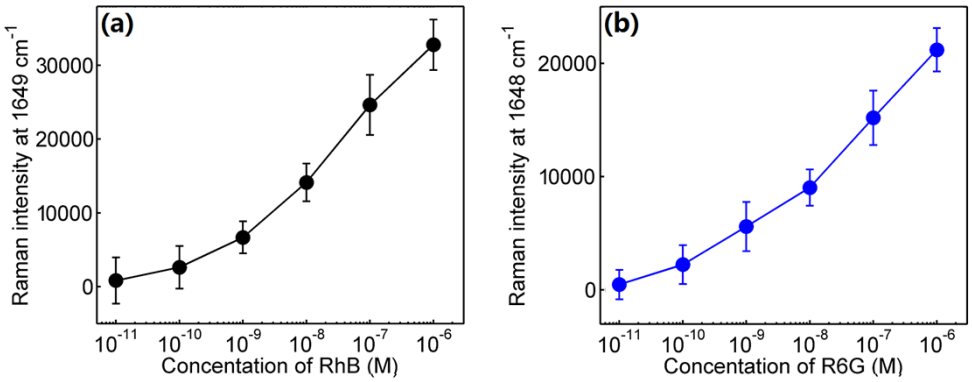

Fig. S6 The intensity of SERS signal versus the concentration of (a) RhB at 1649 cm^{-1} and (b) R6G at 1648 cm^{-1}.

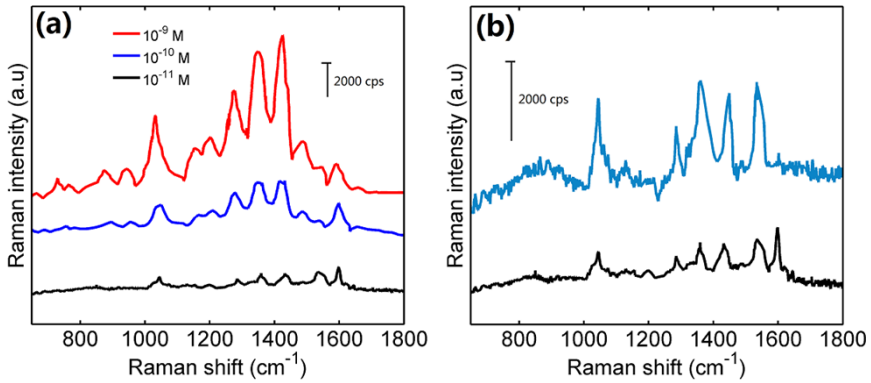

Fig. S7 (a) SERS spectra of TNT on 8 nm Au/1LG/8 nm Ag structure with 3 different molecular concentrations. (b) Raman spectra of 10^{-1} M TNT on quartz substrate (upper curve) and 10^{-11} M on 8 nm Au/1LG/8 nm Ag structure (bottom curve), respectively.

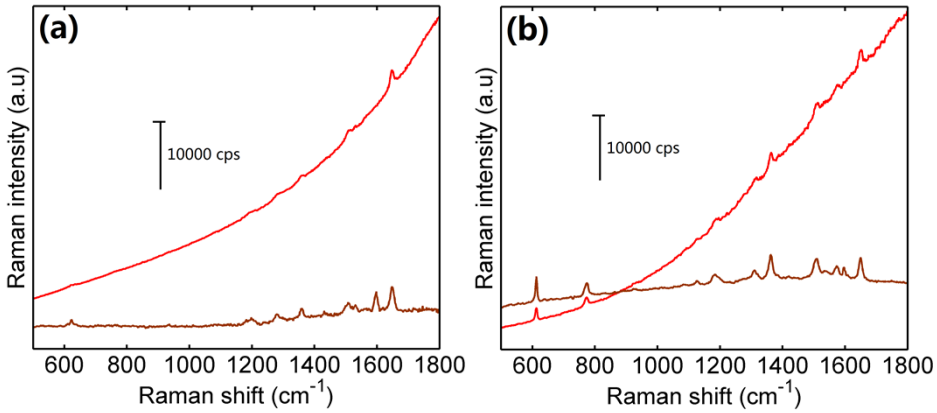

Fig. S8 Raman spectra of (a) RhB and (b) R6G on different substrates with different concentrations. Raman spectra of 10^{-1} M on quartz substrate (upper curves) and 10^{-10} M on 8 nm Au/1LG/8 nm Ag structure (bottom curves), respectively.

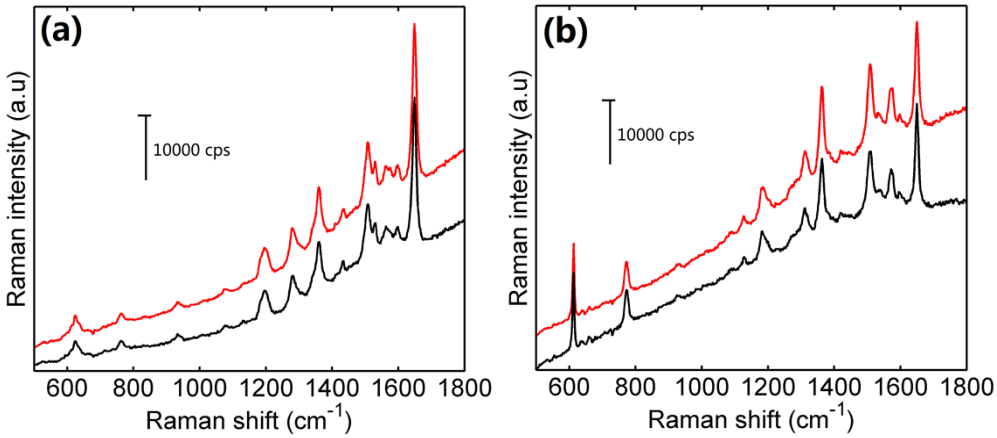

Fig. S9 SERS spectra of 10^{-7} M (a) RhB and (b) R6G on 8 nm Au/1LG/8 nm Ag films measured after two days (red lines) and two months (black lines) since the samples were prepared.

Fig. S10 Raman spectra of RhB on 8 nm Au/8 nm Ag/Ag structure with molecular concentration varying from 10^{-11} M to 10^{-13} M.